RSC Advances

PAPER

View Article Online
View Journal | View Issue

Cite this: *RSC Adv.*, 2020, **10**, 24663

Improvement in the thermoelectric performance of highly reproducible n-type $(Bi,Sb)_2Se_3$ alloys by Cl-doping†

Nadra Nasir,‡[a] Kyu Hyoung Lee,‡[b] Sang-il Kim,[c] Hyun-Sik Kim,[d] Jae-Hong Lim,[e] Liangwei Fu*[a] and Sung Wng Kim*[af]

Received 6th May 2020
Accepted 17th June 2020

DOI: 10.1039/d0ra04065g

rsc.li/rsc-advances

$(Bi,Sb)_2Se_3$ alloys are promising alternatives to commercial n-type $Bi_2(Te,Se)_3$ ingots for low-mid temperature thermoelectric power generation due to their high thermoelectric conversion efficiency at elevated temperatures. Herein, we report the enhanced high-temperature thermoelectric performance of the polycrystalline Cl-doped $Bi_{2-x}Sb_xSe_3$ (x = 0.8, 1.0) bulks and their sustainable thermal stability. Significant role of Cl substitution, characterized to enhance the power factor and reduce the thermal conductivity synergetically, is clearly elucidated. Cl-doping at Se-site of both $Bi_{1.2}Sb_{0.8}Se_3$ and $BiSbSe_3$ results in a high power factor by carrier generation and Hall mobility improvement while maintaining converged electronic band valleys. Furthermore, point defect phonon scattering originated from mass fluctuations formed at Cl-substituted Se-sites reduces the lattice thermal conductivity. Most importantly, spark plasma sintered Cl-doped $Bi_{2-x}Sb_xSe_3$ bulks are thermally stable up to 700 K, and show a reproducible maximum thermoelectric figure of merit, zT, of 0.68 at 700 K.

1. Introduction

Bi_2Te_3-based alloys are the only commercialized thermoelectric materials for solid-state cooling and low-mid temperature (473–873 K) power generation, and their ingot-type materials are widely used due to a high thermoelectric figure of merit ($zT = S^2\sigma T/\kappa_{tot}$, where S, σ, κ_{tot}, and T are the Seebeck coefficient, electrical conductivity, total thermal conductivity, and the absolute temperature, respectively) of about 1.0 near room-temperature.[1] However, ingots of Bi_2Te_3-based alloys have a poor mechanical reliability (fracture strength of ~10 MPa) because of 00*l*-oriented structure weakly bonded by van der Waals forces,[2] which limits their wider applications such as in automobile thermoelectric generator (ATEG). To address this, polycrystalline bulk form materials have been intensively studied, and an improved mechanical strength (~80 MPa) with a higher zT ~1.1 at 300 K has been obtained in micro-grained p-type $Bi_{2-x}Sb_xTe_3$ prepared by ball milling (BM) and spark plasma sintering (SPS).[2] Its n-type counterpart with a comparable mechanical strength and zT is required to construct thermoelectric module with improved mechanical reliability as well as high performance, however, no marked improvement in zT from n-type micro-grained materials was achieved in BMed and SPSed $Bi_2Te_{2.7}Se_{0.3}$ (~0.63 at 300 K).[3] Furthermore, a severe reproducibility problem was also found in this polycrystalline sample owing to the uncontrollable defect structures such as vacancies (Te- or Se-site) and antisite defects. Polycrystalline bulk of n-type $Bi_2Te_{2.7}Se_{0.3}$ with high zT (~0.98 at 300 K) and improved reproducibility has been demonstrated by combining a cold deformation and a hot extrusion benefitting from precise control of point defects,[4] however, a simpler and yet easily scalable approach is always sought after.

Bi_2Se_3 is a narrow-bandgap layered semiconductor (space group $R\bar{3}m$-D_{3d}^5) with tetradymite structure and it has singly degenerate conduction band. The conduction band minimum (CBM) is observed at the center of the Brillouin zone (Γ-point) and the second conduction band is located 150–250 meV (Z-point) above the CBM,[5–7] thus the zT of pristine Bi_2Se_3 is very low (<0.1 at 300 K) mainly due to low S (~−40 μV K^{-1} at 300 K).[8] High κ_{tot} ~2.4 W m^{-1} K^{-1} at 300 K is another reason for the low zT of Bi_2Se_3. Very recently, Te-free $(Bi,Sb)_2Se_3$-based alloys have been received attention as promising alternatives to $Bi_2(Te,Se)_3$-based alloys especially for low-mid temperature power

[a]*Department of Energy Science, Sungkyunkwan University, Suwon 16419, South Korea. E-mail: fulw@skku.edu; kimsungwng@skku.edu*

[b]*Department of Materials Science and Engineering, Yonsei University, Seoul 03722, South Korea*

[c]*Department of Materials Science and Engineering, University of Seoul, Seoul 02504, South Korea*

[d]*Department of Materials Science and Engineering, Hongik University, Seoul 04066, South Korea*

[e]*Department of Materials Science and Engineering, Gachon University, Seongnam 13120, South Korea*

[f]*Center for Integrated Nanostructure Physics, Institute of Basic Science, Suwon 16419, South Korea*

† Electronic supplementary information (ESI) available. See DOI: 10.1039/d0ra04065g

‡ These authors contributed equally to this study.

generation applications. High zT values of ~1.0 and ~1.4 were obtained at 800 K in micro-grained I- and Br-doped $BiSbSe_3$, respectively.[5,9] One main origin of the high thermoelectric performance of these compounds was the simultaneous improvement of electronic (enlarged S) and thermal transport properties (reduced lattice thermal conductivity (κ_{lat})) due to a structural transition.[5] A phase transition triggered the convergence of conduction band resulting in largely increased density of states (DOS) effective mass (m_d^*). Additionally, κ_{lat} was reduced due to the phonon softening and substantial lattice anharmonicity benefitting from weakened interchain interaction in orthorhombic phase. The high zTs were obtained by enhanced power factor ($S^2\sigma$) of I- and Br-doped $BiSbSe_3$ (by an order of magnitude), resulted from the increase in carrier concentration (n_c). However, intrinsic drawbacks of I- and Br-doped $BiSbSe_3$, which included solubility limit of I (~3 at%) and Hall mobility (μ_H) deterioration with Br doping, should be resolved to enhance the low σ value (<300 S cm^{-1} at 300 K) in order to increase the efficiency of the thermoelectric power generation module. Moreover, the thermal stability and reproducibility of high-temperature thermoelectric performance was still elusive, demanding a clear criterion for the temperature limit of the module.

Chlorine (Cl) is a commonly used doping element especially at Se-site of various selenides such as In_4Se_{3-x}, PbSe, $AgPb_{18}SbSe_{20}$, and $SnSe_2$ to increase n_c.[10–13] Moreover, a large difference in atomic mass between Se (M_{Se} = 78.971) and Cl (M_{Cl} = 35.45) is advantageous to further reduce κ_{lat} by mass-defect phonon scattering. In this work, we fabricated the polycrystalline bulks of Cl-doped $Bi_{2-x}Sb_xSe_3$ (x = 0.8, 1.0) and evaluated their electronic and thermal transport properties in an effort to develop $(Bi,Sb)_2Se_3$-based alloys with high σ and zT, at the same time. We found that Cl was an effective doping element to facilitate the carrier transport in $Bi_{1.2}Sb_{0.8}Se_3$, thus high μ_H of ~27.3 cm^2 V^{-1} s^{-1} was observed even in highly Cl-doped $Bi_{1.2}Sb_{0.8}Se_{2.76}Cl_{0.24}$ with high n_c (~9.0 × 10^{19} cm^{-3}). Compared to I-doped $Bi_{1.2}Sb_{0.8}Se_{2.91}I_{0.09}$ (σ ~80 S cm^{-1} and zT ~0.53 at 700 K),[5] higher σ (~165 S cm^{-1} at 700 K) and higher zT (~0.67 at 700 K) were obtained in $Bi_{1.2}Sb_{0.8}Se_{2.76}Cl_{0.24}$. Moreover, we confirmed the thermal stability of the sample by a cyclic measurement.

2. Experimental methods

High purity elements of bismuth (Bi shot, 99.99%, 5N Plus), antimony (Sb shot, 99.99%, 5N Plus), selenium (Se shot, 99.99%, iTASCO), and antimony trichloride ($SbCl_3$ crystalline, 99.99%, Sigma Aldrich) were used as starting raw materials. Stoichiometric ($BiSbSe_{3-y}Cl_y$ (y = 0, 0.12, 0.18, 0.24) and $Bi_{1.2}Sb_{0.8}Se_{3-z}Cl_z$ (z = 0, 0.12, 0.18, 0.24, 0.3)) amount of these materials was weighted and sealed into a quartz tube under vacuum (~10^{-3} Pa), and the mixtures were melted at 1173 K for 12 h. After melting, the quartz tubes were water quenched and annealed at 673 K for 48 h. The acquired ingots were pulverized into powders *via* BM, and compacted bulks (13 mm in diameter and 11 mm in thickness) were fabricated by using SPS for 2 min at 773 K under a pressure of 40 MPa.

Phase formation behavior in SPSed bulks was analyzed by X-ray diffraction (XRD, SmartLab (9 kW), Rigaku, Japan) with CuKα radiation (λ = 1.5418 Å). The microstructures of the fractured surface of the SPSed bulks were investigated by scanning electron microscopy (SEM, JSM-7600F, JEOL, Japan). The temperature dependences of S and σ were measured using a commercial measurement system (ZEM-3, Ulvac-Riko, Japan) from 300–700 K under a He atmosphere. The κ_{tot} ($=D \times C_p \times \rho$, where D, C_p, and ρ are the thermal diffusivity, specific heat capacity, and the density, respectively) was calculated from the separate measurement of D and ρ. Temperature-dependent D was measured by laser flash method (TC-1200RH, Ulvac-Riko, Japan) from 300–700 K under a vacuum and ρ was measured by the Archimedes principle (MD-300S, Alfa Miracle, Japan). Temperature dependence of C_p was estimated from the reported values.[5] The rectangular bar-type sample (10 mm × 3 mm × 3 mm) and square plate-type sample (10 mm × 10 mm × 1 mm) were cut in a plane perpendicular and parallel to the SPS press direction, respectively. In this manner, electronic (S, σ) and thermal (D) transport properties can be measured in the same direction. The Hall coefficient (R_H) was measured by the van der Pauw method *via* a commercial Hall effect measurement system (8400 Series, LakeShore, USA) at room temperature. The n_c and μ_H were calculated by $n_c = e^{-1}R_H^{-1}$ and $\mu_H = \sigma R_H$.

3. Results and discussion

In the present study, we selected two different matrixes; (1) $BiSbSe_3$ with an orthorhombic phase and (2) $Bi_{1.2}Sb_{0.8}Se_3$ with orthorhombic and rhombohedral phases.[5] Fig. 1a shows the XRD patterns for $BiSbSe_{3-y}Cl_y$ samples. All the peaks can be indexed as a pure orthorhombic structure of Sb_2Se_3 without any secondary phases, suggesting the Cl substitution at Se-site. Structure factors including lattice parameters of $BiSbSe_3$-based compounds with orthorhombic phase (Fig. S1†) and those of $Bi_{1.2}Sb_{0.8}Se_3$-based compounds with mixed (orthorhombic and rhombohedral) phases (Fig. S3†) were extracted by the Rietveld refinement (GSAS II suite) after refinements with different structural models at the condition of convergence with the best pattern match. The slight decrease in lattice parameters (a and c) of $BiSbSe_3$ after the Cl doping is another evidence for Cl substitution due to the smaller ionic radius of Cl^- (167 pm) when compared to that of Se^{2-} (184 pm) (Fig. S1†). On the other hand, as reported in the previous report,[14] both orthorhombic and rhombohedral phases are clearly detected in $Bi_{1.2}Sb_{0.8}Se_{3-z}Cl_z$ samples as shown in Fig. 1b. Peaks for the rhombohedral structure of Bi_2Se_3 were observed at 2θ ~18.58° and ~29.35°. The strongest intensity of (402) indicates the preferred crystal orientation generated during the SPS process. Oriented grain structure is also found in SEM images for the fractured surface of SPSed $Bi_{1.2}Sb_{0.8}Se_{3-z}Cl_z$ (Fig. 1c and S2†). The mole fraction of rhombohedral phase estimated by Rietveld refinement is about 0.74, and this value does not show significant change with Cl doping contents (see the Table S1†). And slight decrease in cell volume by Cl-doping is observed in orthorhombic phase (Fig. S3†). Cl-related impurity phase

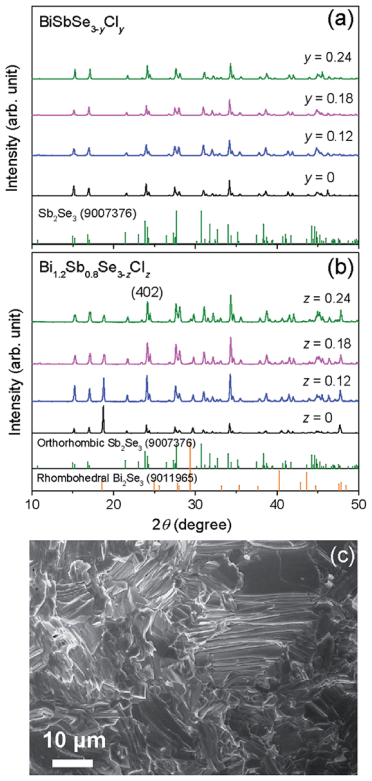

Fig. 1 XRD patterns for the SPSed bulks of (a) $BiSbSe_{3-y}Cl_y$ ($y = 0$, 0.12, 0.18, 0.24) and (b) $Bi_{1.2}Sb_{0.8}Se_{3-z}Cl_z$ ($z = 0$, 0.12, 0.18, 0.24). (c) SEM image for the fractured surface of $Bi_{1.2}Sb_{0.8}Se_{2.76}Cl_{0.24}$.

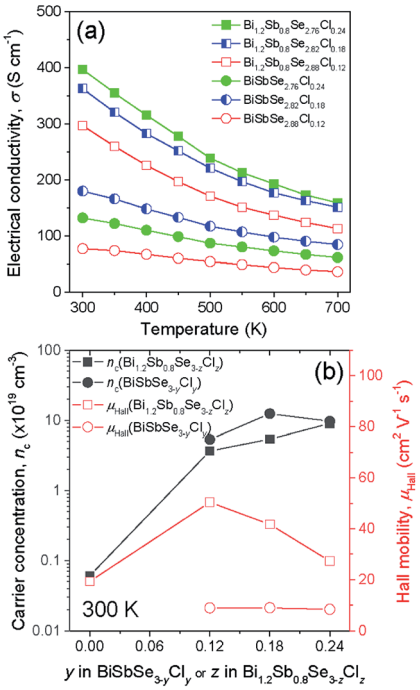

Fig. 2 (a) Temperature dependence of electrical conductivity and (b) carrier concentration and Hall mobility for $BiSbSe_{3-y}Cl_y$ ($y = 0.12$, 0.18, 0.24) and $Bi_{1.2}Sb_{0.8}Se_{3-z}Cl_z$ ($z = 0.12$, 0.18, 0.24).

(Bi_3Se_4Cl) was observed in $Bi_{1.2}Sb_{0.8}Se_{2.7}Cl_{0.3}$, suggesting that the solubility limit of Cl for Se-site is about 8 at% in $Bi_{1.2}Sb_{0.8}Se_3$ (Fig. S4†).

The temperature dependences of σ for both $BiSbSe_{3-y}Cl_y$ ($y = 0.12$, 0.18, 0.24) and $Bi_{1.2}Sb_{0.8}Se_{3-z}Cl_z$ ($z = 0.12$, 0.18, 0.24) samples are plotted in Fig. 2a. All thermoelectric transport properties (σ, S, and κ) are measured perpendicular to SPS pressing direction since the electrical transport is dominant along the in-plane direction. The σ values of $BiSbSe_3$ and $Bi_{1.2}Sb_{0.8}Se_3$ are effectively increased by Cl-doping. Interestingly, the σ values of Cl-doped $Bi_{1.2}Sb_{0.8}Se_3$ are higher than those of Cl-doped $BiSbSe_3$ in the whole measured temperature range. The σ values of the $BiSbSe_{2.76}Cl_{0.24}$ are 132 S cm^{-1} and 61.2 S cm^{-1} at 300 K and 700 K, respectively, while those of $Bi_{1.2}Sb_{0.8}Se_{2.76}Cl_{0.24}$ are 397 S cm^{-1} and 159 S cm^{-1} at 300 K and 700 K, respectively. To clarify this, we estimated the n_c and μ_H of both Cl-doped $BiSbSe_3$ and $Bi_{1.2}Sb_{0.8}Se_3$ at 300 K (Fig. 2b). The improvement in σ by Cl-doping is resulted from the increase of μ_H as well as n_c both in $BiSbSe_3$ and $Bi_{1.2}Sb_{0.8}Se_3$. It is noted that μ_H values of Cl-doped $Bi_{1.2}Sb_{0.8}Se_3$ are much higher than those of Cl-doped $BiSbSe_3$. The μ_H values of $BiSbSe_{3-y}Cl_y$ ($y = 0.12$, 0.18, 0.24) at 300 K is ranged from 8.44 to 9.01 cm^2 V^{-1} s^{-1}, whereas that of $Bi_{1.2}Sb_{0.8}Se_{2.88}Cl_{0.12}$ is ~50.4 cm^2 V^{-1} s^{-1}. Moreover, the μ_H value of highly Cl-doped $BiSbSe_{2.76}Cl_{0.24}$ is retained in value about 27.3 cm^2 V^{-1} s^{-1} despite of the high n_c ~9.0×10^{19} cm^{-3}. This high μ_H has been also reported in I-doped $Bi_{1.2}Sb_{0.8}Se_3$.[5]

Unexpected difference between electronic transport properties of Cl-doped $Bi_{1.2}Sb_{0.8}Se_3$ and those of I-doped $Bi_{1.2}Sb_{0.8}Se_3$ is observed in S. Fig. 3a depicts the temperature dependences of S for both $BiSbSe_{3-y}Cl_y$ ($y = 0.12$, 0.18, 0.24) and $Bi_{1.2}Sb_{0.8}Se_{3-z}Cl_z$ ($z = 0.12$, 0.18, 0.24) samples. The S values of the all samples are negative in the whole measured temperature range, indicating n-type semiconductors. The large $|S|$ values of Cl-doped $BiSbSe_3$ samples due to the convergence of conduction band by phase transition are well demonstrated both in I-doped and Br-doped $BiSbSe_3$.[5,9] To investigate the change in band structure by Cl-doping especially in $Bi_{1.2}Sb_{0.8}Se_3$, we calculate the m_d^* by using measured S and n_c at 300 K based on the following eqn (1):[1]

$$S = \frac{8\pi^2 k_B^2 T}{3eh^2}\left(\frac{\pi}{3n_c}\right)^{2/3} m_d^*, \quad (1)$$

where k_B, e, and h are the Boltzmann constant, elementary charge, and Planck constant, respectively. The m_d^* values are listed in Table 1 together with those for I-doped $BiSbSe_3$ and $Bi_{1.2}Sb_{0.8}Se_3$ samples, which are estimated from eqn (1) by using previously reported data.[5] Large m_d^* values of $1.55m_0$ and $1.67m_0$ are obtained both in $BiSbSe_{2.82}Cl_{0.18}$ and $BiSbSe_{2.91}I_{0.09}$, respectively, with pure orthorhombic phase benefiting from converged electronic band valleys. However, the m_d^* values of Cl-doped $Bi_{1.2}Sb_{0.8}Se_3$ and those of I-doped $Bi_{1.2}Sb_{0.8}Se_3$ are smaller than those of Cl- and I-doped $BiSbSe_3$ mainly due to the large mole fraction of rhombohedral phase (Table S1†) with singly-degenerate conduction band. It is noted that m_d^* value of $Bi_{1.2}Sb_{0.8}Se_{2.76}Cl_{0.24}$ reaches value about $0.90m_0$, which results

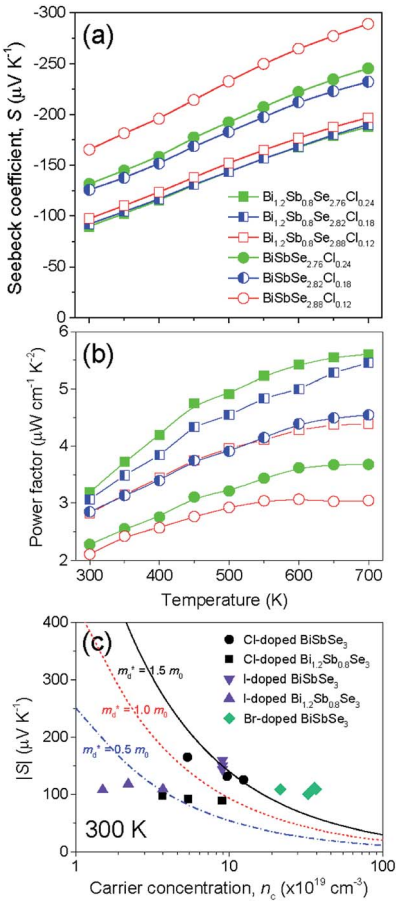

Fig. 3 Temperature dependence of (a) Seebeck coefficient and (b) power factor for $BiSbSe_{3-y}Cl_y$ (y = 0.12, 0.18, 0.24) and $Bi_{1.2}Sb_{0.8}Se_{3-z}Cl_z$ (z = 0.12, 0.18, 0.24). (c) Pisarenko plot for Cl-, I-, and Br-doped $BiSbSe_3$ and Cl- and I-doped $Bi_{1.2}Sb_{0.8}Se_3$ at 300 K.

in a large S even in $Bi_{1.2}Sb_{0.8}Se_3$ systems. Fig. 3c shows the Pisarenko plots (n_c–$|S|$) for both $BiSbSe_{3-y}Cl_y$ (y = 0.12, 0.18, 0.24) and $Bi_{1.2}Sb_{0.8}Se_{3-z}Cl_z$ (z = 0.12, 0.18, 0.24) samples at 300 K. Those for I-doped $BiSbSe_3$, I-doped $Bi_{1.2}Sb_{0.8}Se_3$, and Br-doped $BiSbSe_3$ samples are also shown for comparison.[5,9]

As clearly shown in Fig. 3c, similar value of S is obtained in $Bi_{1.2}Sb_{0.8}Se_{2.76}Cl_{0.24}$ despite of the large increase in n_c when compared to that of I-doped $Bi_{1.2}Sb_{0.8}Se_3$ samples. Resultantly, a maximum power factor values of ~3.19 μW cm^{-1} K^{-2} and ~5.61 μW cm^{-1} K^{-2} at 300 K and 700 K, respectively, are obtained in $Bi_{1.2}Sb_{0.8}Se_{2.76}Cl_{0.24}$ (Fig. 3b), which ensures the enhanced zT especially at higher temperatures. This beneficial characteristic feature for the realization of highly-efficient low-mid temperature thermoelectric power generation system is only found in Cl-doped $Bi_{1.2}Sb_{0.8}Se_3$ among other $(Bi,Sb)_2Se_3$-based alloys.

Fig. 4a shows the temperature dependence of κ_{tot} for $BiSbSe_{3-y}Cl_y$ (y = 0.12, 0.18, 0.24) and $Bi_{1.2}Sb_{0.8}Se_{3-z}Cl_z$ (z = 0.12, 0.18, 0.24) samples. The κ_{tot} values of Cl-doped $Bi_{1.2}Sb_{0.8}Se_3$ are higher than those of Cl-doped $BiSbSe_3$. The room temperature κ_{tot} values of both Cl-doped $BiSbSe_3$ and $Bi_{1.2}Sb_{0.8}Se_3$ are ~0.58–0.62 W m^{-1} K^{-1} and ~0.72–0.83 W m^{-1} K^{-1}, respectively. This is considered to be related to the increased electronic contribution (κ_{ele}) originated from the higher σ of Cl-doped $Bi_{1.2}Sb_{0.8}Se_3$. On the other hand, as shown in Fig. 4a, the κ_{tot} of all the samples gradually decrease with temperature, suggesting the small contribution of bipolar thermal conduction (κ_{bp}). We estimated the κ_{lat} and κ_{ele} by using the relationship of $\kappa_{tot} = \kappa_{ele} + \kappa_{lat}$. Details for the calculation are described in Section 6 of ESI.†

Fig. 4b shows the temperature dependence of κ_{lat} for both Cl-doped $BiSbSe_3$ and $Bi_{1.2}Sb_{0.8}Se_3$. The temperature dependence of κ_{lat} shows roughly $\kappa_{lat} \propto T^{-0.5}$, indicating the additional point defect phonon scattering from the mass difference between host Se (M_{Se} = 78.971) and dopant Cl (M_{Cl} = 35.45) by Cl substituted at Se-site. The κ_{lat} values of Cl-doped $BiSbSe_3$ are lower than those of Cl-doped $Bi_{1.2}Sb_{0.8}Se_3$ mainly due to the soft bonding in orthorhombic phase, however, κ_{lat} reduction effect

Table 1 The density-of-states effective mass (m_d^*) values of Cl-doped $BiSbSe_3$ and $Bi_{1.2}Sb_{0.8}Se_3$. Those of I-doped $BiSbSe_3$ and $Bi_{1.2}Sb_{0.8}Se_3$, which are estimated from the reported data ref. 5, are also shown for comparison

Compositions (nominal)	m_d^* (m_0)	Compositions (nominal)	m_d^* (m_0)
$BiSbSe_{2.88}Cl_{0.12}$	1.17	$BiSbSe_{2.97}I_{0.03}$	1.50
$BiSbSe_{2.82}Cl_{0.18}$	1.55	$BiSbSe_{2.94}I_{0.06}$	1.63
$BiSbSe_{2.76}Cl_{0.24}$	1.38	$BiSbSe_{2.91}I_{0.09}$	1.67
$Bi_{1.2}Sb_{0.8}Se_{2.88}Cl_{0.12}$	0.54	$Bi_{1.2}Sb_{0.8}Se_{2.97}I_{0.03}$	0.33
$Bi_{1.2}Sb_{0.8}Se_{2.82}Cl_{0.18}$	0.66	$Bi_{1.2}Sb_{0.8}Se_{2.94}I_{0.06}$	0.65
$Bi_{1.2}Sb_{0.8}Se_{2.76}Cl_{0.24}$	0.90	$Bi_{1.2}Sb_{0.8}Se_{2.91}I_{0.09}$	0.43

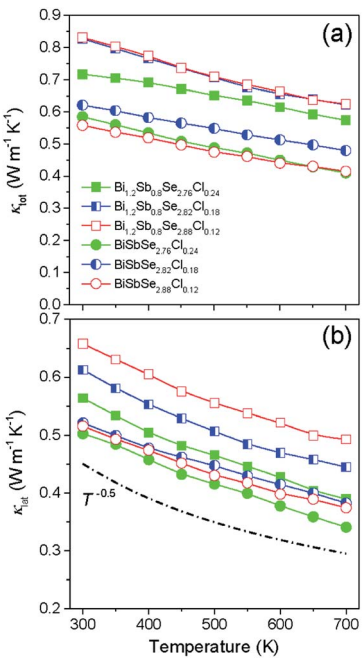

Fig. 4 Temperature dependence of (a) total thermal conductivity and (b) lattice thermal conductivity for $BiSbSe_{3-y}Cl_y$ (y = 0.12, 0.18, 0.24) and $Bi_{1.2}Sb_{0.8}Se_{3-z}Cl_z$ (z = 0.12, 0.18, 0.24).

by Cl-doping is relatively small compared to that of Cl-doped $Bi_{1.2}Sb_{0.8}Se_3$ due to cumulative phonon scattering by soft bonding and point defect. Thus the significantly reduced κ_{lat} ($\sim$0.56 W m^{-1} K^{-1} at 300 K and $\sim$0.39 W m^{-1} K^{-1} at 700 K) is obtained in $Bi_{1.2}Sb_{0.8}Se_{2.76}Cl_{0.24}$ mainly due to the intensified mass-defect phonon scattering. The slightly higher κ_{lat} of $BiSbSe_{2.82}Cl_{0.18}$ than that of $BiSbSe_{2.88}Cl_{0.12}$ is considered to be related with the difference in preferred orientation (Fig. 1b).

Fig. 5a and b show the temperature dependent zT of $BiSbSe_{3-y}Cl_y$ (y = 0.12, 0.18, 0.24) and that of $Bi_{1.2}Sb_{0.8}Se_{3-z}Cl_z$ (z = 0.12, 0.18, 0.24), respectively. The Cl-doping effectively enhances the zT both in $BiSbSe_3$ and $Bi_{1.2}Sb_{0.8}Se_3$ due to improvement of electronic and thermal transport properties. High zT of Cl-doped $BiSbSe_3$ with pure orthorhombic phase is mainly due to the enlarged m_d^* benefitting from the increased valley degeneracy and flattened band, which results in a larger S. Reduced κ_{lat} by the bond softening in orthorhombic phase is another origin for high zT of Cl-doped $BiSbSe_3$. On the other hand, higher zT found in Cl-doped $Bi_{1.2}Sb_{0.8}Se_3$ despite of high rhombohedral phase fraction ($\sim$0.74) is attributed to the simultaneous improvement of electronic (enlarged m_d^* and improved μ_H) and thermal (reduced κ_{lat}) transport properties by Cl-doping. The highly-reproducible maximum zT reaches in value about 0.68 $\pm$ 0.04 at 700 K for three different $Bi_{1.2}Sb_{0.8}Se_{2.76}Cl_{0.24}$ samples. Moreover, high σ values of 397 S cm^{-1} at 300 K and 159 S cm^{-1} at 700 K make this material a promising candidate for practical applications.

We verify the thermal stability of $Bi_{1.2}Sb_{0.8}Se_{2.76}Cl_{0.24}$ *via* the cyclic measurement of zT within temperature range from 300 K to 700 K (Fig. 6a) and remeasurement of power factor after annealing at 800 K for 10 h (Fig. 6b). Fig. 6a and b indicate that the Cl-doped $Bi_{1.2}Sb_{0.8}Se_3$ alloys are chemically stable up to 700 K.

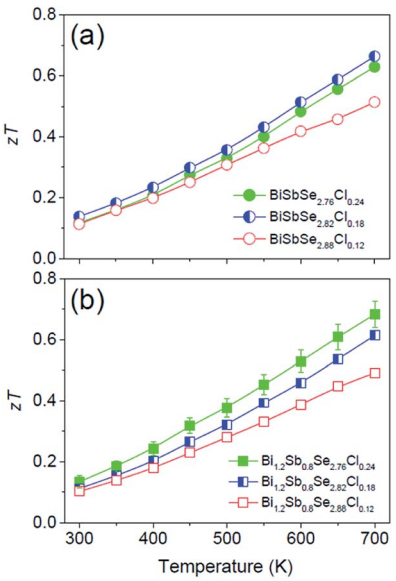

Fig. 5 Temperature dependence of dimensionless figure of merit zT for (a) $BiSbSe_{3-y}Cl_y$ (y = 0.12, 0.18, 0.24) and (b) $Bi_{1.2}Sb_{0.8}Se_{3-z}Cl_z$ (z = 0.12, 0.18, 0.24).

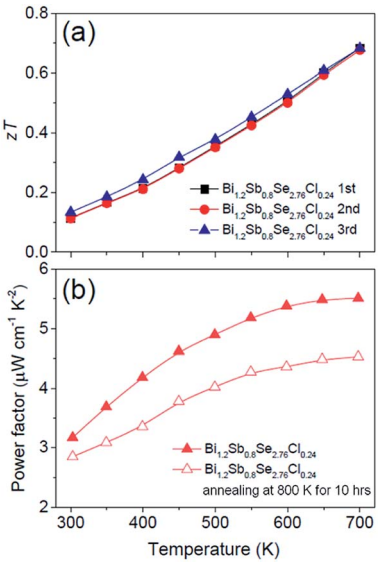

Fig. 6 (a) Cyclic measurement of temperature dependence of dimensionless figure of merit zT for $Bi_{1.2}Sb_{0.8}Se_{2.76}Cl_{0.24}$. (b) Variation in temperature dependent power factor of $Bi_{1.2}Sb_{0.8}Se_{2.76}Cl_{0.24}$ after annealing at 800 K for 10 h.

4. Conclusions

In summary, temperature dependent thermoelectric transport properties of Te-free Cl-doped $BiSbSe_3$ and $Bi_{1.2}Sb_{0.8}Se_3$ are systematically investigated. Improved Seebeck coefficient and electrical conductivity are simultaneously obtained due to the enlarged density-of-states effective mass by high content Cl-doping ($\sim$8 at%), while maintaining intrinsic high mobility of $Bi_{1.2}Sb_{0.8}Se_3$-based alloys. This provides the optimized power factor of $\sim$5.61 μW cm^{-1} K^{-2} at 700 K. Additionally, despite of the weaker phonon scattering owing to decreased bond softening effect in $Bi_{1.2}Sb_{0.8}Se_3$ compared to that in $BiSbSe_3$, lattice thermal conductivity is effectively reduced in value about 0.39 W m^{-1} K^{-1} at 700 K by 8 at% Cl-doping from the intensified mass-defect phonon scattering. This synergetic effect contributes to a high electrical conductivity of $\sim$159 S cm^{-1} and the high zT $\sim$0.68 at 700 K.

Conflicts of interest

There are no conflicts to declare.

Acknowledgements

This work was supported by the National Research Foundation of Korea (NRF) grant funded by the Korean Government (MSIP) (NRF-2017R1A2B3011949) and Global Frontier Program through the Global Frontier Interface Materials (GFHIM) of the National Research Foundation of Korea (NRF) funded by the Ministry of Science, ICT & Future Planning (2013M3A6B1078870).

References

1 G. J. Snyder and E. S. Toberer, *Nat. Mater.*, 2008, **7**, 105.
2 J. Jiang, L. Chen, S. Bai, Q. Yao and Q. Wang, *Scr. Mater.*, 2005, **52**, 347.
3 K. H. Lee, S. I. Kim, H. Mun, B. Ryu, S. M. Choi, H. J. Park, S. Hwang and S. W. Kim, *J. Mater. Chem. C*, 2015, **3**, 10604.
4 S. J. Jung, B. H. Lee, B. K. Kim, S. S. Lim, S. K. Kim, D. I. Kim, S. O. Won, H. H. Park, J. S. Kim and S. H. Baek, *Acta Mater.*, 2018, **150**, 153.
5 S. Wang, Y. Sun, J. Yang, B. Duan, L. Wu, W. Zhang and J. Yang, *Energy Environ. Sci.*, 2016, **9**, 3436.
6 S. K. Mishra, S. Satpathy and O. Jepsen, *J. Phys.: Condens. Matter*, 1997, **9**, 461.
7 P. Larson, V. A. Greanya, W. C. Tonjes, R. Liu, S. D. Mahanti and C. G. Olson, *Phys. Rev. B: Condens. Matter Mater. Phys.*, 2002, **65**, 85108.
8 W. Liu, K. C. Lukas, K. McEnaney, S. Lee, Q. Zhang, C. P. Opeil, G. Chen and Z. Ren, *Energy Environ. Sci.*, 2013, **6**, 552.
9 X. Liu, D. Wang, H. Wu, J. Wang, Y. Zhang, G. Wang, S. J. Pennycook and L. D. Zhao, *Adv. Funct. Mater.*, 2019, **29**, 106558.
10 J. S. Rhyee, K. Ahn, K. H. Lee, H. S. Ji and J. H. Shim, *Adv. Mater.*, 2011, **23**, 2191.
11 Q. Zhang, H. Wang, W. Liu, H. Wang, B. Yu, Q. Zhang, Z. Tian, G. Ni, S. Lee, K. Esfarjani, G. Chen and Z. Ren, *Energy Environ. Sci.*, 2012, **5**, 5246.
12 Q. Zhang, Y. Lan, S. Yang, F. Cao, M. Yao, C. Opeil, D. Broido, G. Chen and Z. Ren, *Nano Energy*, 2013, **2**, 1121.
13 S. I. Kim, S. Hwang, S. Y. Kim, W. J. Lee, D. W. Jung, K. S. Moon, H. J. Park, Y. J. Cho, Y. H. Cho, J. H. Kim, D. J. Yun, K. H. Lee, I. Han, K. Lee and Y. Sohn, *Sci. Rep.*, 2016, **6**, 19733.
14 V. G. Kuznetsov, K. K. Palkina and A. A. Reshchikova, *Izv. Akad. Nauk SSSR, Neorg. Mater.*, 1968, **4**, 670.